Propagation in the transverse tubular system and voltage dependence of calcium release in normal and *mdx* mouse muscle fibres

Christopher E. Woods, David Novo, Marino DiFranco, Joana Capote and Julio L. Vergara

Department of Physiology, UCLA School of Medicine, Los Angeles, CA 90095, USA

Using a two-microelectrode voltage clamp technique, we investigated possible mechanisms underlying the impaired excitation–contraction coupling in skeletal muscle fibres of the *mdx* mouse, a model of the human disease Duchenne muscular dystrophy. We evaluated the role of the transverse tubular system (T-system) by using the potentiometric indicator di-8 ANEPPS, and that of the sarcoplasmic reticulum (SR) Ca^{2+} release by measuring Ca^{2+} transients with a low affinity indicator in the presence of high EGTA concentrations under voltage clamp conditions. We observed minimal differences in the T-system structure and the T-system electrical propagation was not different between normal and *mdx* mice. Whereas the maximum Ca^{2+} release elicited by voltage pulses was reduced by ∼67% in *mdx* fibres, in agreement with previous results obtained using AP stimulation, the voltage dependence of SR Ca^{2+} release was identical to that seen in normal fibres. Taken together, our data suggest that the intrinsic ability of the sarcoplasmic reticulum to release Ca^{2+} may be altered in the *mdx* mouse.

(Received 25 April 2005; accepted after revision 23 August 2005; first published online 25 August 2005)
Corresponding author J. L. Vergara: Department of Physiology, UCLA School of Medicine, Los Angeles, CA 90095, USA. Email: jvergara@mednet.ucla.edu

Duchenne muscular dystrophy (DMD), the most common debilitating genetic disorder affecting boys, has been shown to be caused by mutations in the dystrophin gene, located on the X-chromosome, which leads to the improper expression of the protein dystrophin (Hoffman *et al.* 1987*a*; Emery, 2002). A great deal of our understanding of the physiological impact of dystrophin comes from experimental evidence obtained from studies of the *mdx* mouse, an animal model of DMD that also lacks the expression of dystrophin in the dystrophin-associated glycoprotein (DAG) complex (for a review see: Gillis, 1999). Importantly, muscle fibres from both DMD patients and *mdx* mice display reduced specific active force development (Watchko *et al.* 2002). Under physiological conditions, impairment in SR Ca^{2+} release in response to an action potential (AP) could cause skeletal muscle fibre weakness since Ca^{2+} is the trigger for contraction and the dependence of tension development on myoplasmic free Ca^{2+} concentration is very steep (Godt, 1974; Fink *et al.* 1990). Previous publications have investigated this possibility by comparing AP-evoked Ca^{2+} transients between normal and *mdx* fibres. However, the results are controversial. Some authors report only minimal differences in the kinetic properties and no significant differences in the amplitude of transients recorded from normal and *mdx* muscles (Turner *et al.* 1988; Head, 1993; Tutdibi *et al.* 1999). In contrast, our group recently found that the action potential (AP)-evoked Ca^{2+} release is significantly depressed in *mdx* fibres (Woods *et al.* 2004). While these latter results are important because they provide a physiological foundation for muscle weakness in *mdx* fibres, the use of AP stimulation did not permit us to elucidate which step(s) in the excitation–contraction (EC) coupling process underlie the reduction in Ca^{2+} release.

The membranes of the T-system are responsible for the radial propagation of depolarization in skeletal muscle fibres (Adrian *et al.* 1969) and are involved in the transduction process at specialized junctions called triads (Franzini-Armstrong, 1972; Dulhunty, 1989) where the voltage gradient triggers Ca^{2+} release from the SR. It is currently believed that the voltage sensor for this transduction process is the dihydropyridine receptor (DHPR) located in the T-system membrane which, by interacting with the ryanodine receptor (RyR) in the SR membrane, initiates the Ca^{2+} release (for a review see: Dulhunty *et al.* 2002). Indeed, since SR Ca^{2+} release through the RyR is the final result of this complex multi-step process, impairment in any component could result in the overall decrease in SR Ca^{2+} release that we previously observed in fibres from *mdx* mice (Woods *et al.* 2004). In this paper, we investigated potential alterations in two critical components of the EC coupling process:

 DOI: 10.1113/jphysiol.2005.089318

the structural and electrical properties of the T-system as measured with the potentiometric indicator di-8 ANEPPS (Kim & Vergara, 1998*a*,*b*), and the voltage dependence of the actual Ca^{2+} release flux from the SR, as measured with the low affinity indicator Oregon-Green BAPTA 488-5N (OGB-5N) in the presence of high EGTA concentrations (Song *et al.* 1998; Woods *et al.* 2004). It is conceivable that the absence of dystrophin in the surface membrane (Cullen *et al.* 1990) results in alterations of the T-system properties since these are structurally and functionally interconnected membrane compartments (Rayns *et al.* 1968; Adrian *et al.* 1969; Zampighi *et al.* 1975). However, our results demonstrate that while there is impairment in the SR Ca^{2+} release in *mdx* fibres, it does not arise from alterations in the T-system structure and function, but is constrained to the post-transduction level, indicating a limitation in the ability of the SR to release Ca^{2+} in response to voltage changes.

Methods

Isolation of muscle fibres

All experiments were carried out according to the guidelines laid out by the local UCLA Animal Care Committee. Single muscle fibres were enzymatically isolated from flexor digitorum brevis (FDB) muscles dissected from normal (C57BL/10SnJ) and *mdx* (C57BL/10ScSn-mdx/J) mice (Jackson Laboratories, ME, USA). This muscle has been reported to be composed mostly of fast-twitch (type II) fibres (Parry & Parslow, 1981; Raymackers *et al.* 2000). All experiments were done in 8- to 18-week-old normal and postnecrotic *mdx* mice (McArdle *et al.* 1995). Mice were deeply anaesthetized with halothane (loss of righting reflex) and killed by cervical dislocation. Once excised, the muscles were either dissociated immediately or stored in cold (∼5°C) Tyrode solution and dissociated within 30 min. No differences were observed in the data from fibres in either case.

The dissociation protocol used to isolate single muscle fibres was identical to that previously described (Woods *et al.* 2004). Briefly, isolated FDB muscles were pinned to the bottom of 5 cm Sylgard-coated Petri dishes and incubated in dissociating solution (see below) in a shaking bath at 37°C for 45 min. Collagenase activity was stopped by washing the muscle with 0 Mg^{2+}–0 Ca^{2+} Tyrode solution at 37°C. The muscle mass was gently sucked in and out of a fire-polished Pasteur pipette until muscle fibres were isolated. The fibres were then incubated for a period of 30 min in L-15 media supplemented with 0.1 mg ml^{-1} penicillin–streptomycin and maintained in an O_2-saturated environment at 25°C. Only fibres that responded to external electrical stimulation with twitches were used. In all the experiments, fibres were maintained at slack length.

Solutions

Chemicals, enzymes, proteins, anaesthetics, toxins, culture media and antibiotics were from Sigma (St Louis, MO, USA), while calcium and potentiometric dyes were from Molecular Probes (Eugene, OR, USA). All solutions were adjusted to pH 7.2 and to an osmolality of 300 mosmol (kg $H_2O)^{-1}$. The solute composition (mM, unless otherwise stated) of the solutions were:

K^+ internal solution: 140 potassium aspartate; 20 K-Mops; 5 $MgSO_4$, 5 Na_2-phosphocreatine, 5 K-ATP, 5 dextrose, 2.5 glutathione, 20 EGTA-K, 10 $CaCl_2$ and 0.1 mg ml^{-1} creatine phosphokinase (CPK).

Cs^+ internal solution: 110 caesium aspartate; 20 Mops; 5 $MgSO_4$, 5 Na_2-phosphocreatine, 5 Tris-ATP, 2.5 glutathione, 5 dextrose, 20 EGTA-Cs, 10 $CaCl_2$ and 0.1 mg ml^{-1} CPK.

The free [Ca^{2+}] of both internal solutions was measured to be 63 ± 6 nM.

Tyrode solution: 145 NaCl, 2.5 KCl, 2 $CaCl_2$, 1 $MgCl_2$, 10 Na-Mops, 10 dextrose.

Dissociating solution: 0 Mg^{2+}–0 Ca^{2+} Tyrode solution supplemented with 262 units ml^{-1} of collagenase Type IV and 0.5 mg ml^{-1} of bovine serum albumin.

0 Na^+ Tyrode solution: 125 *N*-methyl-D-glucamine, 2.5 KCl, 10 Mops, 2 $CaCl_2$, 10 dextrose, 1 $MgCl_2$, 10 TEA acetate, 0.5 $CdCl_2$, 200 nM TTX. The pH was adjusted by titration with methane sulphonic acid.

Potassium sulphate solution: 120 K_2SO_4, 10 K-Mops.

Two-photon confocal and DIC imaging

FDB muscle fibres were stained with the potentiometric dye di-8 ANEPPS (5 μM in Tyrode solution for 30 min) and transferred to an optical chamber (DiGregorio *et al.* 1999) placed on the stage of a Leica SP MP two-photon laser scanning confocal microscope (TPLSCM) equipped with a Ti : sapphire tuneable laser. Fibres were imaged using a ×100, 1.4 NA oil immersion objective. The dye was excited at 980 nm and the fluorescence emission was selected with a 560–700 nm bandpass filter. Fluorescence and differential interference contrast (DIC) images were acquired consecutively at several axial planes separated by 5 μm in order to generate a stack of image sections. Each image was acquired at a resolution of 1024 pixels × 1024 pixels. Images were analysed using Image/J (NIH image, USA).

Electrophysiology

A two-microelectrode amplifier (TEV-200A, Dagan, Minneapolis, MN, USA) was used for both current and voltage clamp experiments. Current clamp experiments were performed as previously described (Woods *et al.* 2004). Briefly, the fibres were impaled with two

microelectrodes located close to the centre of the fibres and separated by ~40 μm. The voltage recording microelectrodes had resistances of 20–30 MΩ when filled with 3 M KCl. The current injection microelectrodes had resistances of 30–40 MΩ when filled with internal solutions and were used to passively load the fibres with the Ca^{2+} dye and EGTA. In addition the current electrode was used to deliver holding current and pulses as required to maintain the resting potential and to stimulate the fibres to elicit APs, respectively. For voltage clamp experiments, selected fibres were rendered passive by placing them in 0 Na^+ Tyrode solution for a period of at least 30 min (in an O_2-saturated environment) before microelectrode impalement. The microelectrodes were placed ~10 μm apart, which permitted the establishment of stable voltage clamp pulses to within 95% of the command step in 60 μs. We verified that membrane potential changes were maintained within ~97% of that detected by the voltage recording electrode at distances greater than 100 μm from it.

Calcium transients

The $[Ca^{2+}]$ changes evoked by electrical stimulation were measured using the salt form of the Ca^{2+} indicator OGB-5N, dissolved in internal solutions at a concentration of 500 μM. The equilibrium dissociation constant (K_d) and the F_{max}/F_{min} ratio (R) of OGB-5N were determined *in vitro* using protocols similar to those described elsewhere (Escobar *et al.* 1997; Nagerl *et al.* 2000; Woods *et al.* 2004). For the particular batch of OGB-5N (lot no. 34B2-1) used in this work, K_d and R were 48 ± 7 μM and 11 ± 0.26, respectively.

Global fluorescence transients evoked either by AP or voltage clamp stimulation were recorded using an inverted microscope (Nikon Diaphot) equipped with a × 60, 0.98 NA objective, and a fluorescence cube consisting of a 488/30 nm bandpass excitation filter, a 510 nm dichroic mirror and a 540 nm long pass filter. The illumination spot was limited to about 30 μm, centred with respect to the fibre diameter, and midway between the tips of both microelectrodes. Emitted light was focused on a pin photodiode (HR008, UDT, Hawthorne, CA, USA) connected in photovoltaic configuration to the integrating head-stage of a patch clamp amplifier (Model 200B, Axon Instruments). This light recording system permits rapid detection of optical signals with optimal signal-to-noise ratio (Escobar *et al.* 1994, 1997). The fluorescence transients were normalized with respect to the resting fluorescence in $\Delta F/F$ units and characterized according to parameters previously described (Vergara & DiFranco, 1992; DiFranco *et al.* 2002; Woods *et al.* 2004). We determined that the resting fluorescence of OGB-5N recorded in the populations of normal and *mdx* fibres was not different.

To characterize the voltage dependence of Ca^{2+} release, the peak $\Delta F/F$ of the OGB-5N fluorescence transients was plotted as a function of the membrane voltage, and the data fitted to single (eqn (1)) and double (eqn (2)) Boltzmann distributions, according to the following expressions:

$$\left(\frac{\Delta F}{F}\right)_{peak} = \frac{\left(\frac{\Delta F}{F}\right)_{max}}{1 + e^{-\frac{V_m - \Psi}{k}}} \quad (1)$$

where $\left(\frac{\Delta F}{F}\right)_{max}$ is the maximal $(\Delta F/F)_{peak}$, Ψ is the half-maximum voltage, V_m is the membrane potential and k is the slope.

$$\left(\frac{\Delta F}{F}\right)_{peak} = \frac{\left(\frac{\Delta F}{F}\right)_{max\,1}}{1 + e^{-\frac{V_m - \Psi 1}{k1}}} + \frac{\left(\frac{\Delta F}{F}\right)_{max\,2}}{1 + e^{-\frac{V_m - \Psi 2}{k2}}} \quad (2)$$

where the numbers indicate the separate matching components of each individual Boltzmann in the double fit.

Predictions of the OGB-5N fluorescence transients were performed using a single compartment model as described elsewhere (Woods *et al.* 2004), but with the following changes:
(a) The flux (eqn (5)) in Woods *et al.* (2004) was replaced by the following expression:

$$J(t) = J_T\left(1 - e^{\frac{-t}{\tau_{on1}}}\right)^4 e^{\frac{-t}{\tau_{off1}}} + J_S\left(1 - e^{\frac{-t}{\tau_{on2}}}\right) \quad (3)$$

where J_T is the amplitude of a transient component of the total calcium release flux and J_S is the amplitude of a steady component of the total calcium release flux.
(b) The free $[Mg^{2+}]$ was set to an initial resting value of 600 μM and allowed to vary during model simulations.
(c) Troponin C (TnC, 240 μM) and parvalbumin (900 μM) were included in the mathematical model (Johnson *et al.* 1994; Maughan & Godt, 1999; Novo *et al.* 2003). The association and dissociation kinetic rate constants for Ca^{2+} binding by TnC were 0.15 μM^{-1} ms^{-1} and 0.45 ms^{-1}, respectively (Johnson *et al.* 1994; Baylor & Hollingworth, 1998). For parvalbumin, the kinetic rate constants for Ca^{2+} binding were 0.025 μM^{-1} ms^{-1} and 0.7 ms^{-1}, and for Mg^{2+} binding were 1.5×10^{-5} μM^{-1} ms^{-1} and 3×10^{-3} ms^{-1}, respectively. The interaction between Mg^{2+} and Ca^{2+} followed the scheme described elsewhere (Novo *et al.* 2003).

Optical detection of T-system membrane potentials

The staining procedures for potentiometric studies were similar to those described elsewhere (Kim & Vergara, 1998*a*). Briefly, fibres were stained for 1 h with 2–5 μM

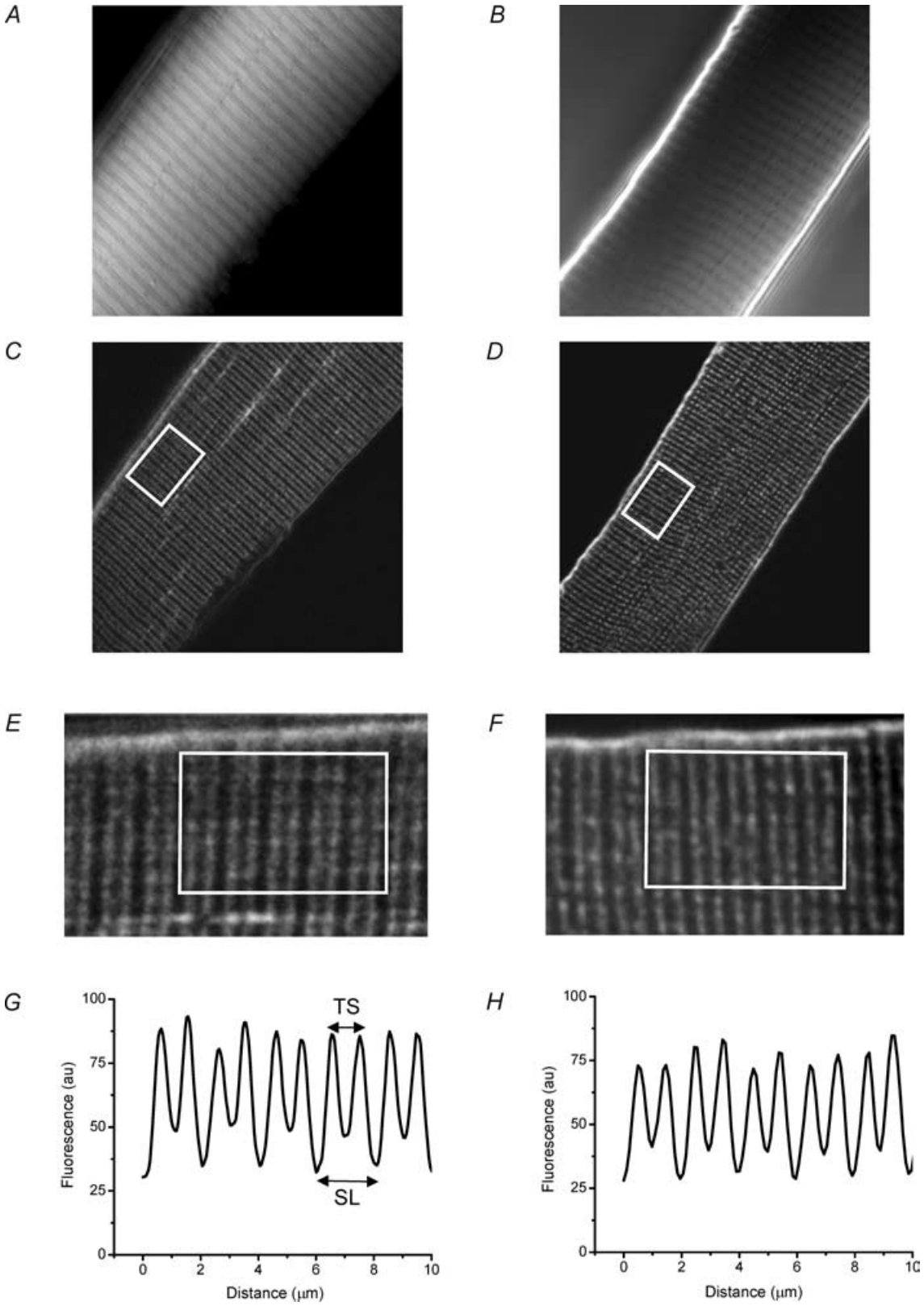

Figure 1. Differential interference contrast (DIC) and two-photon laser scanning confocal microscope (TPLSCM) images of normal and *mdx* fibres stained with di-8 ANEPPS

A and *B*, DIC images of flexor digitorum brevis (FDB) fibres from normal (13 weeks old) and *mdx* (15 weeks old) mice, respectively. *C* and *D*, TPLSCM images from the same fibres as in *A* and *B*, respectively. The image plane was the same as in *A* and *B*. *E* and *F*, enlarged view (× 3 magnification) of equivalent areas of the fibres, including the

di-8 ANEPPS dissolved in isotonic K_2SO_4 solution before mounting them on the chamber. T-system potentiometric signals, associated with action potentials or the application of voltages pulses, were recorded using the same optical system described above for global detection of Ca^{2+} transients, except that the fluorescence cube configuration consisted of a 488/30 nm excitation filter, a 505 nm dichroic mirror and a 600 nm long pass filter, as previously described (Kim & Vergara, 1998*a*).

Statistics

For TPSLCM images, the average sarcomere length (SL) and T-tubule spacing (TS) for each fibre were obtained from rectangular areas comprising many sarcomeres and compared between fibres. For AP-evoked signals, kinetic parameters and amplitudes were determined from a minimum of 10 individual AP-evoked transients per fibre as previously described (Woods *et al.* 2004). For voltage clamp experiments, comparison of parameters between fibres was done by analysing optical records at corresponding voltage pulses. The data are presented as mean ± standard error of the mean (S.E.M.). Student's unpaired two-population *t* test assuming unequal variance was used to compare the mean fibre values between *mdx* and normal mice. *P* values are given in the text.

Results

Given the putative role of the DAG complex in structuring muscle membrane systems (Gillis, 1999), we wished to determine if the absence of dystrophin had any impact on the structural and physiological features of the T-system, and thereby play a role in the impaired AP-elicited SR Ca^{2+} release of these fibres (Woods *et al.* 2004). Accordingly, we obtained DIC and TPLSCM images of live muscle fibres stained with di-8 ANEPPS (see Methods). Panels *A* and *B* in Fig. 1 are DIC images from a single *z*-axis plane within a normal and an *mdx* fibre, respectively. Both images depict the typical interference bands that characterize skeletal muscle fibres. Panels *C* and *D* are the corresponding di-8 ANEPPS fluorescence images obtained using TPLSCM for the same focal planes in Fig. 1*A* and *B*, respectively. The parallel bands of high fluorescence intensity in the TPLSCM images, which run perpendicular to the sarcolemma in the focal planes of Fig. 1*C* and *D*, correspond to di-8 ANEPPS staining of the T-tubules. In the magnified views in Fig. 1*E* and *F*, it can be observed that the T-tubules are organized in a double row per sarcomere pattern, a well-known feature of mammalian skeletal muscle fibres that has been reported with electron microscopy (Franzini-Armstrong *et al.* 1988; Dulhunty, 1989) and with confocal fluorescence microscopy (Krolenko *et al.* 1995; Lannergren *et al.* 1999).

From TPLSCM images like those shown in Fig. 1*C* and *D* (as expanded in Fig. 1*E* and *F*), we generated average fluorescence profiles which give us quantitative information about the spacing of the consecutive T-tubules (TS) and the sarcomere length (SL). Figure 1*G* and *H* are representative fluorescence profiles obtained from the white boxed regions shown in Fig. 1*E* and *F*, respectively. From profiles like these, we calculated values of 2.0 ± 0.02 μm (mean ± S.E.M.) and 0.9 ± 0.02 μm, for SL and TS, respectively, for normal fibres, and 2.1 ± 0.03 and 0.9 ± 0.02 μm, respectively, for dystrophic fibres ($n = 5$ *mdx* fibres from 2 mice; $n = 4$ normal fibres from 2 mice).

Although the above image analysis shows that the gross structural features of the T-system are not significantly altered in *mdx* mice, the important question to answer is whether the functional integrity of this membrane system is preserved between normal and *mdx* fibres. To this end, we recorded simultaneously the AP, known to reflect the voltage changes predominantly across the surface membrane, and the corresponding T-system fluorescence signals in normal and *mdx* fibres stained with di-8 ANEPPS and loaded intracellularly with high EGTA concentrations to arrest contraction (K^+ internal solution, see Methods). Figure 2*A* and *B* shows superimposed scaled records of the T-system AP (noisy trace) and the surface membrane AP (smooth trace) from normal and *mdx* muscle fibres, respectively. Note that, for convenience, fluorescence transients are shown as upward deflections, despite the fact that at the wavelengths used (see Methods), an increase in transmembrane potential represents a decrease in di-8 ANEPPS fluorescence. It should be noted that, in contrast with what has been reported in frog skeletal muscle fibres (Kim & Vergara, 1998*a*,*b*), the time course of the optical transients from both mammalian muscle fibres matches closely (without delay) the electrical recording of the surface AP. Table 1 summarizes the properties of the surface AP and of di-8 ANEPPS transients recorded from normal and *mdx* fibres. It can be concluded that there are no significant differences in the AP propagation at the levels of the surface and T-system membranes between normal and dystrophic fibres.

The absence of a delay between the optical transient and the AP (as described above) suggests that unlike the situation in amphibian fibres (Kim & Vergara, 1998*a*), the possibility exists in mammalian fibres to rapidly charge the T-system membrane capacitance using voltage clamp steps. To investigate this, we recorded the T-system

white rectangles shown in *C* and *D*, respectively. Both images were filtered with a FFT 2-pixel bandpass filter (Image/J). *G* and *H*, average intensity profiles, plotted as a function of the longitudinal position, of areas enclosed within white rectangles in *E* and *F*, respectively. TS is T-tubule spacing; SL is sarcomere length; au, arbitrary units. The length of the long side of the white rectangle represents 10 μm.

Table 1. Properties of surface membrane action potential (AP) and T-system transients

	Surface membrane AP		T-system transient		
	Amplitude (mV)	FDHM (ms)	$(dV/dt)_{max}$ ($V\ s^{-1}$)	$(\Delta F/F)_{peak}$ (%)	FDHM (ms)
Normal fibres	113 ± 8	2.0 ± 0.8	327 ± 93	6.7 ± 1.0	2.0 ± 0.02
Mdx fibres	109 ± 6	2.3 ± 1.4	273 ± 82	6.5 ± 0.8	2.1 ± 0.03

The above abbreviations are defined as follows: FDHM, full duration at half-maximum; $(dV/dt)_{max}$, maximum rate of rise of the AP. Results were obtained from $n = 17$ fibres from 3 normal mice, and $n = 9$ fibres from 2 *mdx* mice.

fluorescence signals elicited in response to voltage steps in fibres stained with di-8 ANEPPS under voltage clamp conditions. Fibres were rendered electrically passive by using ion replacement and conductance blockers (Cs^+ internal solution and 0 Na^+ Tyrode external solution; see Methods) that prevent a non-linear behaviour due to the activation of T-system conductive pathways (Vergara & Bezanilla, 1981; Heiny & Vergara, 1982; Heiny *et al.* 1983; Vergara *et al.* 1983; Heiny & Jong, 1990; Kim & Vergara, 1998*a*,*b*). Figure 3*A* and *B* show optical transients recorded in response to step depolarizations 10 ms in duration (see legend for amplitudes) from a normal and an *mdx* fibre, respectively. As suspected from the AP signals shown above, the time course of the voltage response of the T-system (optical transient) is remarkably similar to that imposed at the surface membrane. Note the similarity between the electrical and optical signals for steps to +40 mV (Fig. 3*A* and *B*) where the time course of both traces reaches a steady state within ~100 μs of the pulse onset. In order to characterize the voltage dependence of the di-8 ANEPPS signals, we plotted the steady state fluorescence changes (expressed in $\Delta F/F$ units) as a function of the surface membrane potential as imposed by a family of voltage clamp pulses (10 ms) applied from −90 mV. Pooled data from several normal and *mdx* fibres are shown in Fig. 3*C* and *D*, respectively. Each data point represents the average fluorescence over an interval of 5 ms after reaching the steady state. A slope of $-0.06\Delta F/F$ per 100 mV was found from linear regressions of data obtained from both types of fibres. With this information, we estimate that the amplitudes of the T-system APs for the optical traces in Fig. 2*A* and *B* are approximately 117 and 112 mV, respectively.

A principal role of the T-system in skeletal muscle physiology is the inward propagation of the AP to the triads in order to enable the voltage-dependent transduction process involved in evoking SR Ca^{2+} release. Since *mdx* fibres exhibit a decrease in AP-evoked SR Ca^{2+} release (Woods *et al.* 2004) in the absence of any alteration in the electrical properties of the T-system (Figs 2 and 3, this report), it is possible that the EC coupling process of *mdx* fibres is altered at the level of either the voltage transduction process or the mechanisms involved in Ca^{2+} release of the SR itself. In order to test whether the voltage dependence of this transduction is impaired in *mdx* muscle fibres, we recorded evoked SR Ca^{2+} release in voltage clamped fibres by using high [EGTA] and the low affinity Ca^{2+} indicator OGB-5N (Cs^+ internal solution and 0 Na^+ Tyrode external solution; see Methods). It has been shown previously that under

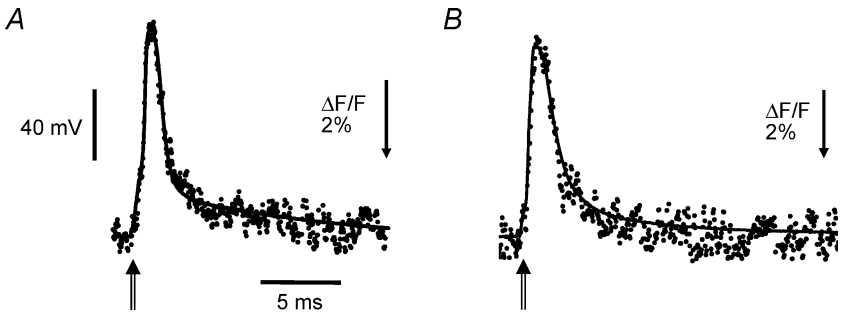

Figure 2. AP and di-8 ANEPPS transients from normal and *mdx* FDB fibres
A, AP (continuous trace) and evoked di-8 ANEPPS fluorescence transient (dotted trace) from a normal FDB muscle fibre. Resting membrane potential, −93 mV. AP parameters: amplitude, 128 mV; FDHM, 1.5 ms. Optical transient parameters: $(\Delta F/F)_{peak}$, 7%; FDHM, 1.32 ms. Fibre diameter, 31 μm. *B*, AP (continuous trace) and evoked di-8 ANEPPS fluorescence transient (dotted trace) from a dystrophic FDB fibre. Resting membrane potential, −89 mV. AP parameters: amplitude, 110 mV; FDHM, 1.84 ms. Optical transient parameters: $(\Delta F/F)_{peak}$, 6.7%; FDHM, 1.84 ms. Fibre diameter: 28 μm. The double-stemmed arrows indicate the point of stimulation. The optical signals are averages of 5 consecutive records. Fibres were loaded with K^+ internal solution and the external solution was Tyrode. Temperature: 22°C.

these conditions the global fluorescence transients can closely track the time course of the SR Ca^{2+} release flux (Song *et al.* 1998; Woods *et al.* 2004). Figure 4*A* shows representative OGB-5N fluorescence signals elicited by 10 ms voltage pulses in a normal fibre. Figure 4*B* shows the electrical records of the membrane potential steps to the values indicated in the figure legend. It can be seen that steps to membrane potentials ≥ -40 mV were required to elicit detectable Ca^{2+} signals. Larger depolarizations elicited progressively bigger Ca^{2+} signals until, for membrane potentials > 0 mV, their amplitude reached a plateau as is typically observed in skeletal muscle EC coupling. The kinetics of the Ca^{2+} signals in response to voltage clamp depolarizations were also dependent on the amplitude of the step. Smaller depolarizations evoked a slow rising phase towards a plateau which lasted the length of the pulse while larger depolarizations elicited OGB-5N transients which displayed a rapid rising phase to a peak, followed by a decay phase ($\tau \sim 4$ ms) to a lower steady value. It can be appreciated that there is a measurable delay from the onset of the voltage pulse to the initiation of the Ca^{2+} transient. For the largest depolarizations, the minimum delay observed was $\sim$0.5 ms, which is meaningful given that the settling time of the voltage clamp is less than 0.1 ms (see Fig. 3).

Figure 5 shows representative voltage clamp results from a normal (Fig. 5*A*) and a dystrophic (Fig. 5*B*) fibre, both loaded with a Cs^+ internal solution containing 20 mM total EGTA and OGB-5N with 0 Na^+ Tyrode solution in the external bath. The voltage steps corresponding to each OGB-5N fluorescence transient in Fig. 5*A* and *B* were identical. As can be appreciated, the amplitude of the Ca^{2+} signals is smaller at each corresponding voltage in the *mdx* compared with the normal fibre. We wished to quantify the voltage dependence of SR Ca^{2+} release in order to see if the voltage sensitivity of the release process was altered or whether only the peak release in response to stimulation was altered in *mdx* fibres. In Fig. 6*A*, the voltage dependence of the average $(\Delta F/F)_{peak}$ from seven normal fibres (4 mice) and seven *mdx* fibres (7 mice) is shown. Both data sets in Fig. 6*A* could be fitted accurately by using double Boltzmann distributions

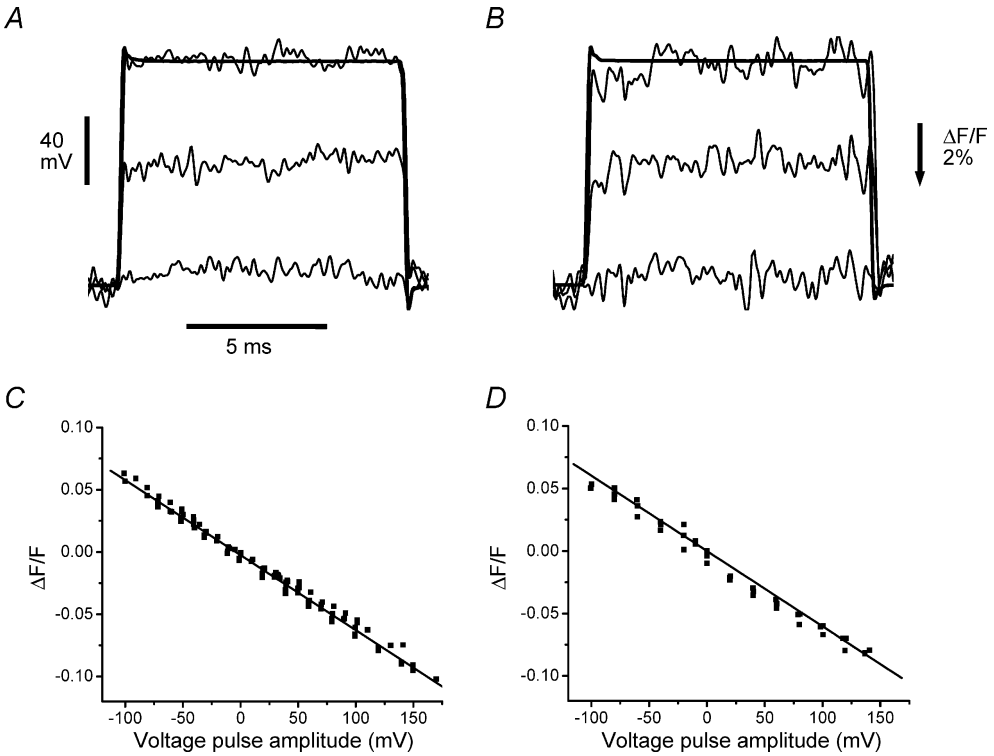

Figure 3. Di-8 ANEPPS transients in response to step voltage pulses in normal and *mdx* fibres
A and *B*, di-8 ANEPPS transients (noisy traces) elicited in normal FDB (*A*) and *mdx* fibres (*B*) by step depolarizations to -80, -20 and $+40$ mV. The holding potential was -90 mV. Fibre diameters: *A*, 29 μm; *B*, 31 μm. Voltage records of the pulses to $+40$ mV are shown superimposed with the corresponding di-8 ANEPPS transients in the normal and the *mdx* fibre. The optical and electrical signals were filtered at 5 kHz. *C* and *D*, scatter plots of the steady-state di-8 ANEPPS transients recorded in normal (*C*) and *mdx* fibres (*D*) in response to step voltage pulses as in *A* and *B*. Optical data (in $\Delta F/F$ units) is plotted as a function of the relative voltage step amplitude (abscissa) from a resting potential of -90 mV. Both data sets (normal and *mdx*) were obtained from 3 fibres in 3 different animals. Linear regression fits to the data are shown as continuous lines. Both plots have a correlation factor of -0.99, and a slope of -6% per 100 mV. Internal solution was the Cs^+ internal solution. External solution was 0 Na^+ Tyrode.

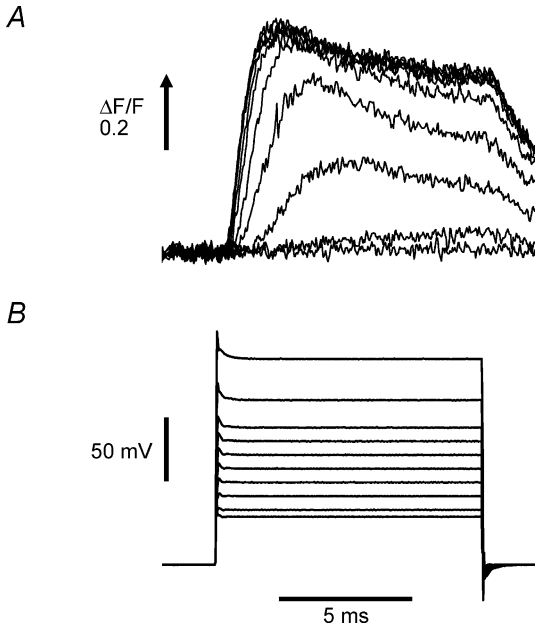

Figure 4. OGB-5N transients elicited by voltage pulses in a normal FDB fibre
A, OGB-5N fluorescence transients were recorded in response to 10 ms voltage steps (from a holding potential of −90 mV) to −55, −50, −40, −30, −20, −10, 0, +10, +30, and +60 mV. *B*, membrane potential records of the pulses described above. The internal solution was Cs^+ internal solution and the external solution was 0 Na^+ Tyrode. Fibre diameter: 30 μm.

(see Methods and Fig. 6*A*), but single Boltzmann fits were sufficiently accurate to provide for estimations of the asymptotic values of the $(\Delta F/F)_{peak}$ voltage dependence. The resulting theoretical curves are shown superimposed with the data in Fig. 6*A*, and the parameters are presented in the figure legend. The voltage dependence of the $(\Delta F/F)_{peak}$ is very steep from −50 mV until it plateaus at ∼0 mV. It should be also noted that the maximal $(\Delta F/F)_{peak}$ values, estimated from the single Boltzmann fits for the largest depolarizations tested, were 0.57 and 0.19 for normal and *mdx* fibres, respectively. These values show a significant depression in the maximal Ca^{2+} release in *mdx* fibres, which amounts to 67 ± 7% of the normal. Data from normal and *mdx* fibres was normalized to their respective maxima and plotted superimposed in Fig. 6*B*. It can be observed that the voltage dependence of the $(\Delta F/F)_{peak}$ between normal and dystrophic fibres does not show significant differences (see legend of Fig. 6*B*).

Discussion

Muscle fibre weakness is a well-known feature of dystrophic animals (for review, see Watchko *et al.* 2002). We recently provided the first evidence demonstrating that SR Ca^{2+} release in response to AP stimulation is significantly reduced in isolated *mdx* muscles fibres (Woods *et al.* 2004). These results were important since they may go towards explaining, at least partially, the muscle weakness observed in *mdx* mice. Nevertheless, the experimental approach used before did not allow us to identify the mechanisms involved in the overall reduction in AP-evoked Ca^{2+} release in *mdx* fibres. In this report, we used a combination of methods aimed to give us further insight into which step(s) of the EC coupling process underlie(s) the impairment in SR Ca^{2+} release in *mdx* fibres.

The T-system is a membrane compartment with a precise geometry likely to be crucial for the physiological role it plays in EC coupling. The absence of dystrophin could alter the 3-D morphology of this membrane compartment. We investigated this possibility *in vivo* by acquiring TPLSCM images from FDB fibres stained with di-8 ANEPPS (Fig. 1*C*–*F*). One advantage of this approach is that it allows interlacing structural observations of the T-system in live fibres with differential interference contrast (DIC) images of the sarcomeric pattern (Fig. 1*A* and *B*). The normal appearance of the sarcomeres can be appreciated in the DIC images of normal and *mdx* fibres after the enzymatic dissociation process. The di-8 ANEPPS fluorescence images from both normal and *mdx* fibres showed a double row of T-tubules per sarcomere, a distinctive feature of mammalian skeletal muscle fibres that has been documented previously (Revel, 1962; Dulhunty, 1989; Krolenko *et al.* 1995; Franzini-Armstrong *et al.* 1998; Lannergren *et al.* 1999). Importantly, there are no major T-system structural differences between normal and *mdx* fibres. In addition, TS distances in unstretched fibres at equal SLs are similar in both strains.

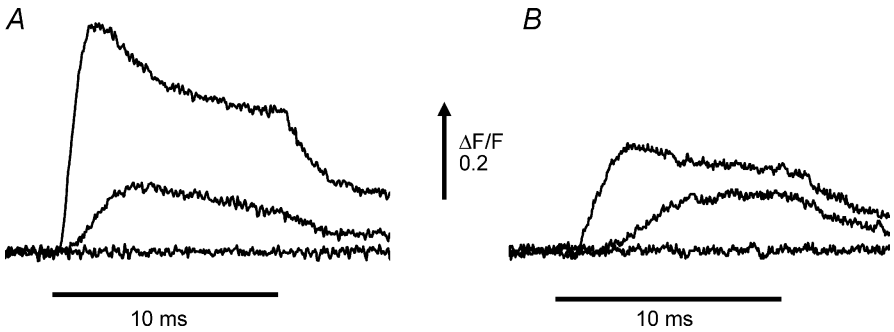

Figure 5. Comparison of OGB-5N transients elicited by voltage clamp pulses in normal and dystrophic FDB fibres
A, OGB-5N transients, recorded from a normal FDB fibre, elicited by voltage steps (from a holding potential of −90 mV) to −60, −40 and 0 mV. Fibre diameter: 32 μm. *B*, OGB-5N transients elicited by identical voltage steps to those in *A*, but from an *mdx* FDB fibre. Fibre diameter: 29 μm. In both cases Cs^+ internal solution and 0 Na^+ Tyrode were used.

Although the FDB fibres from normal and *mdx* mice seem structurally similar, since the T-tubular AP acts as the triggering signal for Ca^{2+} release from the SR, any alteration in T-system physiology would be potentially reflected in an abnormal Ca^{2+} release. With the assumption that di-8 ANEPPS (like other fast potentiometric indicators) reports voltage changes similarly from the surface and the T-system membranes, the fluorescence signal recorded optically in response to AP stimulation is expected to be representative of voltage changes occurring preferentially in the T-system (Heiny & Vergara, 1984; Kim & Vergara, 1998*b*). From structural measurements in mammalian tissue, this membrane compartment is estimated to comprise ~88% of the muscle membrane area (Eisenberg, 1983). However, taking into account the existence of caveolae, capacitance measurements in rat muscles suggest a smaller value of ~71% (Dulhunty *et al.* 1984). Fluorescence signals obtained from disc-shaped regions of illumination within the muscle fibres have been shown to selectively weight the surface membrane contribution depending on the selected location and the depth discrimination of the microscope objective (Kim & Vergara, 1998*b*). In the current experiments, the sectioning power of the 0.98 NA objective (Hiraoka *et al.* 1990) is calculated to minimize spurious contributions outside the illuminated disc to within less than 5% (authors' unpublished results). Thus, the similarity between AP-evoked fluorescence transients in normal and *mdx* mice (Fig. 2 and Table 1) suggest that T-system propagation is not altered in diseased muscle fibres. By applying the calibration curve for the di-8 ANEPPS response to voltage, we calculated that the amplitude of the T-tubule AP was on average 113 mV for normal fibres and 109 mV for *mdx* fibres (see Table 1). This is almost identical to values obtained for the amplitude of the surface AP. In fact, the non-significant 4% decrease in the peak of the surface AP between normal and dystrophic FDB fibres is precisely mirrored by a non-significant 4% decrease in the $(\Delta F/F)_{peak}$ of the potentiometric transients between the two fibre types. Taken altogether, our potentiometric dye results weaken the possibility that fibre damage is a potential cause of the difference in Ca^{2+} release flux between normal and *mdx* fibres.

Previous investigations in amphibian fibres have demonstrated that, under passive conditions, the response of the T-system to step voltage pulses is significantly slower than that at the surface membrane (Heiny & Vergara, 1982; Heiny *et al.* 1983; Ashcroft *et al.* 1985; Kim & Vergara, 1998*a*,*b*), because of the presence of a large access resistance at the mouth of the T-tubules (Adrian & Peachey, 1973; Kim & Vergara, 1998*b*) and a large luminal resistance of the T-tubules (Adrian *et al.* 1969; Ashcroft *et al.* 1985; Kim & Vergara, 1998*b*). In contrast, the results of Fig. 3 show that, using step voltage pulses, it was possible to charge the T-system capacitance almost simultaneously with the surface membrane voltage pulse. Indeed, 95% of the steady state value for the T-system fluorescence was achieved within 0.1 ms, which is significantly faster than

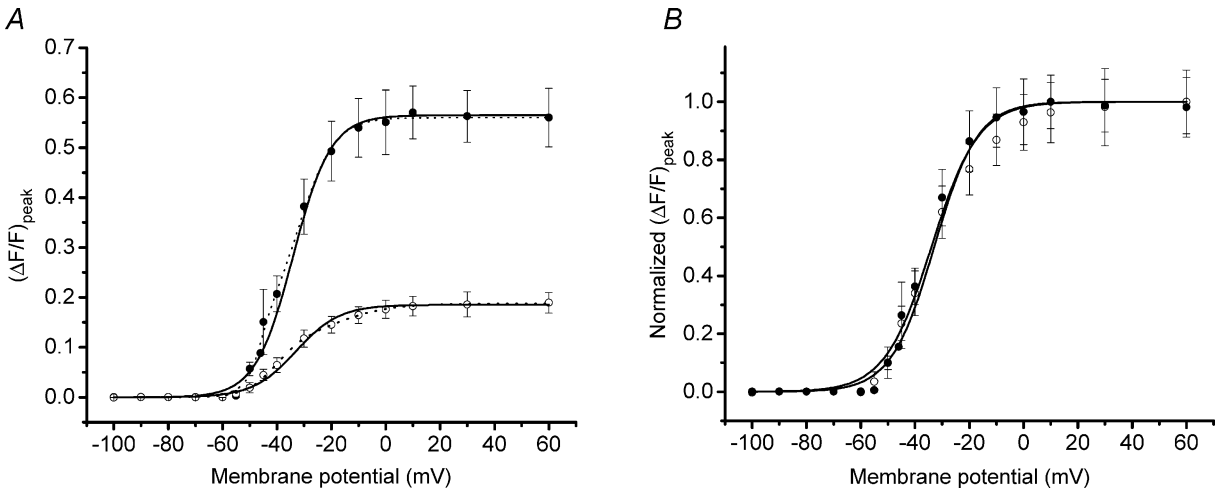

Figure 6. Average voltage-dependent properties of OGB-5N transients from normal and *mdx* FDB fibres
A, average $(\Delta F/F)_{peak}$ of OGB-5N transients plotted as a function of the membrane potential for *mdx* (○) and normal (●) FDB fibres. Bars represent the S.E.M. Data were fitted to single (continuous lines) and double Boltzmann (dashed lines) distributions using eqns (1) and (2) in Methods, respectively. Boltzmann parameters $(\Delta F/F)_{max}$, Ψ (mV) and k (mV) for the single fit are: 0.19 ± 0.02, -32.93 ± 2.53 and 7.97 ± 0.88 for *mdx* fibres and 0.57 ± 0.05, -34.07 ± 2.72 and 6.93 ± 0.62 for normal fibres. Boltzmann parameters $(\Delta F/F)_{max1}$, $(\Delta F/F)_{max2}$, $\Psi 1$, $\Psi 2$, $k1$ and $k2$ for the double fit of the average $(\Delta F/F)_{peak}$ are: 0.12, 0.07, −40.4, −16.64, 5.46 and 9.76 for *mdx* fibres and 0.27, 0.36, −43.79, −30.37, 3.91 and 6.15 for normal fibres. *B*, data sets from *A* were normalized to their corresponding maximal $(\Delta F/F)_{peak}$ and plotted superimposed. Only the single Boltzmann fits are shown.

could be achieved even with the use of supercharging pulse protocols in amphibian cut muscle fibres (Kim & Vergara, 1998*a*,*b*). This finding is compatible with the smaller size of the FDB mammalian fibres (diameters of 25–40 μm used here *versus* 80–120 μm for amphibian fibres), but also with the presence of a smaller access resistance in mammalian fibres, a possibility which needs to be further investigated.

The absence of alterations in both the T-system structure and in the AP generation and conduction in *mdx* fibres, suggested that the mechanism underlying the impaired SR Ca^{2+} release flux is likely to be located either at the voltage transduction process at the triad, or at the level of the SR itself. We investigated these possibilities by studying the voltage dependence of the $\Delta F/F$ transient under voltage clamp conditions. This technique has been used to investigate the voltage dependence of Ca^{2+} release in cut and intact mammalian fibres previously (Delbono & Stefani, 1993; Szentesi *et al.* 1997), but these studies only inferred the voltage dependence of the SR Ca^{2+} release flux from theoretical deconvolutions of the evoked Ca^{2+} transients. In our work, instead, we combined the voltage clamp technique with the use of a low affinity Ca^{2+} indicator and high intracellular [EGTA]. It has been demonstrated previously by our group and others (Song *et al.* 1998; Novo *et al.* 2003; Woods *et al.* 2004) that this approach allows for a direct evaluation of the SR Ca^{2+} release flux from the recorded fluorescence transients. It should be noted that a basic assumption for the validity of flux comparisons between normal and *mdx* fibres is that the *in vivo* Ca^{2+}-binding properties of the indicator are not different for each fibre population. In support of this contention, we have shown that, unlike other Ca^{2+} indicators, the *in vivo* and *in vitro* properties of the salt form of OGB-5N are quite similar (Vergara *et al.* 2001; DiFranco *et al.* 2002). Furthermore, neither equilibrium nor kinetic Ca^{2+}-binding parameters of OGB-5N are significantly affected by major changes in viscosity (attained by varying the concentration of various proteins) of the solution in which the dye is dissolved (Nagerl *et al.* 2000; M. DiFranco & J. L. Vergara, unpublished observations).

Example simulations, using modified flux equations and parameters (see Methods) in the model previously described (Woods *et al.* 2004), are shown in Fig. 7 for the $\Delta F/F$ records in response to depolarizations to 0 mV presented in Fig. 5*A* and *B*. Figure 7*A* and *B* shows the experimental $\Delta F/F$ signals (continuous traces) superimposed with the predicted $\Delta F/F$ (dashed traces) and free [Ca^{2+}] (dotted traces) for normal and *mdx* fibres, respectively. The corresponding calculated Ca^{2+} release fluxes are shown superimposed in Fig. 7*C*. It can be observed that, as previously demonstrated for other EGTA concentrations (Song *et al.* 1998; Novo *et al.* 2003; Woods *et al.* 2004), the time course of the predicted [Ca^{2+}] changes closely matches that of the measured $\Delta F/F$ fluorescence transients. The predicted flux traces in Fig. 7*C* reach peak values of 319 μM ms^{-1} and 150 μM ms^{-1} for the normal and *mdx* fibres, respectively. Thus, a 53% reduction in the Ca^{2+} release flux is matched almost identically by a 52% reduction in the experimental $\Delta F/F$ transients. The importance of this simulation is that under the high [EGTA] conditions used here the voltage dependence of $(\Delta F/F)_{peak}$ for normal and *mdx* fibres closely reflects that of the SR Ca^{2+} release flux. As such, the voltage dependence of the $(\Delta F/F)_{peak}$ shown in Fig. 6 also reflects the voltage dependence of the peak Ca^{2+} release flux. We found that double Boltzmann fits predicted the experimental data better, suggesting the presence of at least two voltage-sensing charge components for the EC coupling process in mammalian skeletal muscle fibres, as we have observed previously for amphibian fibres (Kim & Vergara, 1998*a*). For comparative purposes, however, the single Boltzmann distribution proved sufficient in allowing us to calculate (from the ratio of $(\Delta F/F)_{max}$ in *mdx* with respect to normal fibres) that the average maximal $(\Delta F/F)_{peak}$ is depressed, on average, by ~67% in dystrophic muscles. We conclude therefore that there is a substantial limitation in the ability of the SR to maximally release Ca^{2+} in *mdx* fibres. On this point, our results are at odds with those obtained, also in dissociated FDB fibres, by Collet *et al.* (1999). However, our data demonstrate similar voltage dependences for the peak Ca^{2+} signals in normal and *mdx* fibres, which is in agreement with these authors' findings. It also concurs with a previous report which found no differences in the voltage dependence of charge movement currents between normal and *mdx* fibres (Hollingworth *et al.* 1990).

The modelling approach can be used to make predictions about what to expect from the reduced Ca^{2+} release flux in *mdx* fibres in terms of Ca^{2+} binding to TnC and thus to infer a possible effect on contraction. In order to estimate the time course of formation of the Ca^{2+}–TnC complex in native normal and *mdx* fibres in response to a voltage clamp step, we removed EGTA from the model and solved the model equations using the fluxes shown in Fig. 7*C*. The changes in [Ca^{2+}–TnC] for normal (continuous trace) and *mdx* fibres (dashed trace) are shown in Fig. 7*D*. It can be seen that, while in normal fibres the Ca^{2+} release flux is capable of rapidly driving the formation of the Ca^{2+}–TnC complex such that within ~4 ms its concentration reaches saturating levels, in *mdx* fibres the process evolves more slowly and saturation is only attained after ~9 ms. Based on these results it could be speculated that, in response to prolonged voltage depolarizations, the kinetics of tension development should be different in normal and *mdx* fibres, but they would eventually attain similar steady tension levels. We also used the above single compartment model but with Ca^{2+} release kinetic parameters required to predict OGB-5N Ca^{2+} transients recorded in response to action potential (AP) stimulation (Woods *et al.* 2004). We

found that the ∼46% reduction in peak Ca^{2+} release flux observed in *mdx* fibres with respect to normal controls (Woods *et al.* 2004) predicts a ∼16% drop in the maximal [Ca^{2+}–Tnc] formed (data not shown). This result and those shown in Fig. 7*C* and *D* emphasize the non-linear dependence of the TnC complex formation on the underlying kinetics and amplitude of the Ca^{2+} release flux. More importantly, with the caveat that the Ca^{2+} sensitivity of the contractile apparatus is unchanged (Williams *et al.* 1993), they support the possibility that reported values (in the range of 13–50%) for the reduction in specific twitch tension in *mdx* muscles (Sacco *et al.* 1992; Petrof *et al.* 1993; Hayes & Williams, 1998; Watchko *et al.* 2002) could be accounted for by impairments in the Ca^{2+} release flux. Nevertheless, they may not be compatible with other reports on active twitch tension (Quinlan *et al.* 1992).

The findings in this paper suggest that T-system propagation is functionally unaltered in *mdx* fibres. In addition, as discussed above, the voltage dependence of SR Ca^{2+} release in *mdx* fibres is normal. Moreover, it has been previously reported that the charge movement and the amount of DHPR protein in *mdx* fibres is conserved (Hollingworth *et al.* 1990; Culligan *et al.* 2002). These results argue that the impairment in Ca^{2+} release observed here, and previously (Woods *et al.* 2004), occurs at a post-transduction step at the triads, probably at the level of the SR release flux itself, a possibility supported by other independent lines of evidence (Hoffman *et al.* 1987*b*; Knudson *et al.* 1988; Culligan *et al.* 2002; Friedrich *et al.* 2004). Taken together, the prominent depression in Ca^{2+} release observed in dystrophic fibres could result from either a reduction in the number of operational Ca^{2+} release units, or from a reduction in the ability to release Ca^{2+} by each unit. We are currently focusing on local detection experiments in order to decide this important issue. With that caveat, if we assume that the Ca^{2+} release is uniformly depressed among the Ca^{2+} release units, several options need to be considered. Since the SR Ca^{2+} release

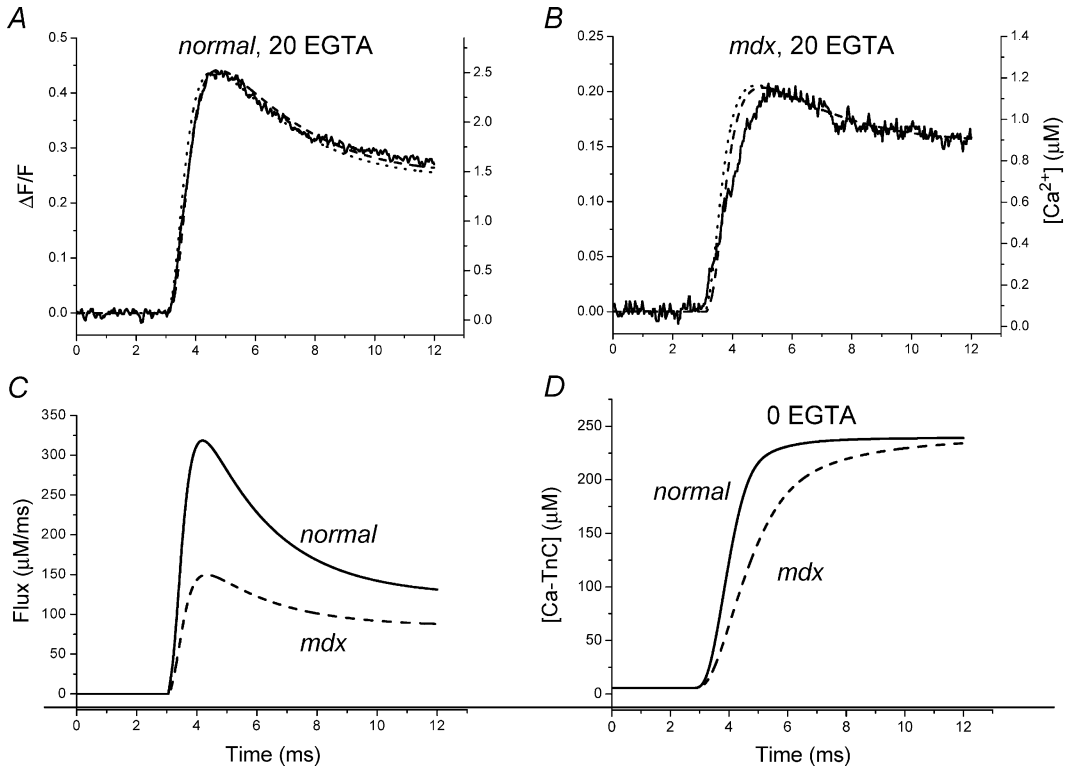

Figure 7. Calcium release flux model simulations
A and *B*, Δ*F*/*F* (dashed lines) and free [Ca^{2+}] (dotted lines) transients generated with a single compartment model after adjustment of flux parameters in order to predict OGB-5N Δ*F*/*F* transients (thick continuous traces). Experimental records (taken from Fig. 5) were obtained in response to a step from −90 to 0 mV in a normal (*A*) and an *mdx* fibre (*B*). *C*, SR calcium release fluxes (see eqn (3) in Methods) for normal (continuous trace) and *mdx* fibres (dashed trace) used to generate traces in *A* and *B*, respectively. The values for the kinetic parameters τ_{on1} (ms), τ_{on2} (ms) and τ_{off1} (ms) were: 0.3, 0.5 and 2.35 for both fibres. The flux amplitudes J_T (μM ms^{-1}) and J_S (μM ms^{-1}) were, respectively, 370 and 123 for the normal fibre, and 130 and 85 for the *mdx* fibre. *D*, time course of Ca^{2+}–TnC formation in normal and *mdx* fibres. [Ca^{2+}–TnC] values were generated by solving the model equations (in the absence of EGTA) while using the flux parameters in panel *C*. Continuous and dashed traces represent normal and *mdx* results, respectively.

flux depends on the single channel permeability of the RyR to Ca^{2+}, the number of RyRs open, and the Ca^{2+} gradient across the SR membrane, alterations in any one of these three properties (or a combination of them) could explain our observations in *mdx* fibres.

The inclusion of very high [EGTA] in the current injection pipette fixes the resting myoplasmic [Ca^{2+}] to a value that approaches the ∼60 nM existing in the pipette (Pusch & Neher, 1988; Woods *et al.* 2004). This experimental manipulation, aside from ensuring an accurate estimate of the Ca^{2+} release flux (Song *et al.* 1998; Woods *et al.* 2004), rules out the possibility that differences in the resting myoplasmic [Ca^{2+}] are responsible for the recording of reduced Ca^{2+} release in *mdx* fibres, e.g. via a [Ca^{2+}]-dependent inactivation mechanism (Simon *et al.* 1991). It has been reported that the *mdx* mouse displays abnormal calsequestrin clustering and that the expression of both the calsequestrin-like Ca^{2+} binding protein (Culligan *et al.* 2002) and sarcalumenin (Dowling *et al.* 2003), two putative Ca^{2+} binding proteins within the SR, is significantly depressed. Furthermore, it has also been reported that the V_{max} of the SR Ca^{2+}-ATPase is reduced by 40% in SR vesicles from *mdx* mice (Kargacin & Kargacin, 1996). Putting this evidence together with our present and previous results (Woods *et al.* 2004), a plausible working hypothesis would be that the total amount of SR Ca^{2+} readily available for release is lower in *mdx* fibres.

An important question that our studies pose is: what is the link between the lack of dystrophin in the sarcolemma and the functional reduction in SR Ca^{2+} release in *mdx* fibres? One possibility is the reported sustained increase in the resting [Ca^{2+}] in *mdx* fibres (Turner *et al.* 1988; Tutdibi *et al.* 1999) putatively resulting from an increased Ca^{2+} leak at the level of the sarcolemma (Turner *et al.* 1991; Tutdibi *et al.* 1999). This could in turn affect the normal levels of expression of RyR and/or other ancillary proteins in the SR membrane. Alternatively, it could be argued that during the enzymatic dissociation process, *mdx* fibres could be more susceptible than normal fibres to undergoing major increases in the basal [Ca^{2+}], which have been reported to irreversibly inhibit SR Ca^{2+} release in skinned fibres by a Ca^{2+}-induced uncoupling mechanism (Lamb *et al.* 1995). This possibility requires the myoplasmic [Ca^{2+}] to reach levels in tens of micromolar (saturating for the mechanical apparatus Wood *et al.* 1978; Williams *et al.* 1993) during several seconds (Lamb *et al.* 1995). However, these conditions are unlikely to occur in the fibres used in our experiments because: (a) the enzymatic dissociation was performed in 0 Ca^{2+}–0 Mg^{2+} Tyrode solution, thus minimizing the probability that Ca^{2+} entry through the sarcolemma could lead to large increases in myoplasmic [Ca^{2+}] in either normal or *mdx* fibres; and (b) the experiments were performed in intact twitching normal and *mdx* fibres (Woods *et al.* 2004) which did not sustain prolonged visible contractures during the dissociation. Fibres that were damaged during the enzymatic dissociation process underwent visible contractures only upon return to Ca^{2+}-containing solutions and were not used in the experiments.

Other potential links between the absence of dystrophin and the results presented in this paper are alterations in the downstream expression of EC coupling proteins induced by various signalling pathways also reportedly found to be affected in *mdx* fibres (McNally *et al.* 1998; Durbeej & Campbell, 2002). Although we cannot explicitly distinguish between causal mechanisms, our experiments highlight the underpinning concept that *mdx* fibres display limitations in their ability to release Ca^{2+} from the SR.

References

Adrian RH, Costantin LL & Peachey LD (1969). Radial spread of contraction in frog muscle fibres. *J Physiol* **204**, 231–257.

Adrian RH & Peachey LD (1973). Reconstruction of the action potential of frog sartorius muscle. *J Physiol* **235**, 103–131.

Ashcroft FM, Heiny JA & Vergara J (1985). Inward rectification in the transverse tubular system of frog skeletal muscle studied with potentiometric dyes. *J Physiol* **359**, 269–291.

Baylor SM & Hollingworth S (1998). Model of sarcomeric Ca^{2+} movements, including ATP Ca^{2+} binding and diffusion, during activation of frog skeletal muscle. *J Gen Physiol* **112**, 297–316.

Collet C, Allard B, Tourneur Y & Jacquemond V (1999). Intracellular calcium signals measured with indo-1 in isolated skeletal muscle fibres from control and *mdx* mice. *J Physiol* **520**, 417–429.

Cullen MJ, Walsh J, Nicholson LV & Harris JB (1990). Ultrastructural localization of dystrophin in human muscle by using gold immunolabelling. *Proc R Soc Lond B Biol Sci* **240**, 197–210.

Culligan K, Banville N, Dowling P & Ohlendieck K (2002). Drastic reduction of calsequestrin-like proteins and impaired calcium binding in dystrophic mdx muscle. *J Appl Physiol* **92**, 435–445.

Delbono O & Stefani E (1993). Calcium transients in single mammalian skeletal muscle fibres. *J Physiol* **463**, 689–707.

DiFranco M, Novo D & Vergara J (2002). Characterization of the calcium release domains during excitation contraction coupling in skeletal muscle fibres. *Pflugers Arch* **443**, 508–519.

DiGregorio DA, Peskoff A & Vergara JL (1999). Measurement of action potential-induced presynaptic calcium domains at a cultured neuromuscular junction. *J Neurosci* **19**, 7846–7859.

Dowling P, Doran P & Ohlendieck K (2003). Drastic reduction of sarcalumenin in Dp427 (dystrophin of 427 kDa)-deficient fibres indicates that abnormal calcium handling plays a key role in muscular dystrophy. *Biochem J* **379**, 479–488.

Dulhunty AF (1989). Feet, bridges, and pillars in triad junctions of mammalian skeletal muscle: their possible relationship to calcium buffers in terminal cisternae and T-tubules and to excitation-contraction coupling. *J Membr Biol* **109**, 73–83.

Dulhunty A, Carter G & Hinrichsen C (1984). The membrane capacity of mammalian skeletal muscle fibres. *J Muscle Res Cell Motil* **5**, 315–332.

Dulhunty AF, Haarmann CS, Green D, Laver DR, Board PG & Casarotto MG (2002). Interactions between dihydropyridine receptors and ryanodine receptors in striated muscle. *Prog Biophys Mol Biol* **79**, 45–75.

Durbeej M & Campbell KP (2002). Muscular dystrophies involving the dystrophin-glycoprotein complex: an overview of current mouse models. *Curr Opin Genet Dev* **12**, 349–361.

Eisenberg BR (1983). Quantitative ultrastructure of mammalian skeletal muscle. In *Handbook of Physiology*, vol. 10, *Skeletal Muscle*, ed. Peachey LD, chap. 3, pp. 73–112. American Physiological Society, Bethesda, MD, USA.

Emery AE (2002). The muscular dystrophies. *Lancet* **359**, 687–695.

Escobar AL, Monck JR, Fernandez JM & Vergara JL (1994). Localization of the site of Ca^{2+} release at the level of a single sarcomere in skeletal muscle fibres. *Nature* **367**, 739–741.

Escobar AL, Velez P, Kim AM, Cifuentes F, Fill M & Vergara JL (1997). Kinetic properties of DM-nitrophen and calcium indicators: rapid transient response to flash photolysis. *Pflugers Arch* **434**, 615–631.

Fink RH, Stephenson DG & Williams DA (1990). Physiological properties of skinned fibres from normal and dystrophic (Duchenne) human muscle activated by Ca^{2+} and Sr^{2+}. *J Physiol* **420**, 337–353.

Franzini-Armstrong C (1972). Studies of the triad. 3. Structure of the junction in fast twitch fibers. *Tissue Cell* **4**, 469–478.

Franzini-Armstrong C, Ferguson DG & Champ C (1988). Discrimination between fast- and slow-twitch fibres of guinea pig skeletal muscle using the relative surface density of junctional transverse tubule membrane. *J Muscle Res Cell Motil* **9**, 403–414.

Franzini-Armstrong C, Protasi F & Ramesh V (1998). Comparative ultrastructure of Ca^{2+} release units in skeletal and cardiac muscle. *Ann N Y Acad Sci* **853**, 20–30.

Friedrich O, Both M, Gillis JM, Chamberlain JS & Fink RH (2004). Mini-dystrophin restores L-type calcium currents in skeletal muscle of transgenic mdx mice. *J Physiol* **555**, 251–265.

Gillis JM (1999). Understanding dystrophinopathies: an inventory of the structural and functional consequences of the absence of dystrophin in muscles of the mdx mouse. *J Muscle Res Cell Motil* **20**, 605–625.

Godt RE (1974). Calcium-activated tension of skinned muscle fibers of the frog. Dependence on magnesium adenosine triphosphate concentration. *J Gen Physiol* **63**, 722–739.

Hayes A & Williams DA (1998). Contractile function and low-intensity exercise effects of old dystrophic (mdx) mice. *Am J Physiol* **274**, C1138–C1144.

Head SI (1993). Membrane potential, resting calcium and calcium transients in isolated muscle fibres from normal and dystrophic mice. *J Physiol* **469**, 11–19.

Heiny JA, Ashcroft FM & Vergara J (1983). T-system optical signals associated with inward rectification in skeletal muscle. *Nature* **301**, 164–166.

Heiny JA & Jong DS (1990). A nonlinear electrostatic potential change in the T-system of skeletal muscle detected under passive recording conditions using potentiometric dyes. *J Gen Physiol* **95**, 147–175.

Heiny JA & Vergara J (1982). Optical signals from surface and T system membranes in skeletal muscle fibers. Experiments with the potentiometric dye NK2367. *J Gen Physiol* **80**, 203–230.

Heiny JA & Vergara J (1984). Dichroic behavior of the absorbance signals from dyes NK2367 and WW375 in skeletal muscle fibers. *J Gen Physiol* **84**, 805–837.

Hiraoka Y, Sedat JW & Agard DA (1990). Determination of three-dimensional imaging properties of a light microscope system. Partial confocal behavior in epifluorescence microscopy. *Biophys J* **57**, 325–333.

Hoffman EP, Brown RH Jr & Kunkel LM (1987*a*). Dystrophin: the protein product of the Duchenne muscular dystrophy locus. *Cell* **51**, 919–928.

Hoffman EP, Knudson CM, Campbell KP & Kunkel LM (1987*b*). Subcellular fractionation of dystrophin to the triads of skeletal muscle. *Nature* **330**, 754–758.

Hollingworth S, Marshall MW & Robson E (1990). Excitation contraction coupling in normal and mdx mice. *Muscle Nerve* **13**, 16–20.

Johnson JD, Nakkula RJ, Vasulka C & Smillie LB (1994). Modulation of Ca^{2+} exchange with the Ca^{2+}-specific regulatory sites of troponin C. *J Biol Chem* **269**, 8919–8923.

Kargacin ME & Kargacin GJ (1996). The sarcoplasmic reticulum calcium pump is functionally altered in dystrophic muscle. *Biochim Biophys Acta* **1290**, 4–8.

Kim AM & Vergara JL (1998*a*). Fast voltage gating of Ca^{2+} release in frog skeletal muscle revealed by supercharging pulses. *J Physiol* **511**, 509–518.

Kim AM & Vergara JL (1998*b*). Supercharging accelerates T-tubule membrane potential changes in voltage clamped frog skeletal muscle fibers. *Biophys J* **75**, 2098–2116.

Knudson CM, Hoffman EP, Kahl SD, Kunkel LM & Campbell KP (1988). Evidence for the association of dystrophin with the transverse tubular system in skeletal muscle. *J Biol Chem* **263**, 8480–8484.

Krolenko SA, Amos WB & Lucy JA (1995). Reversible vacuolation of the transverse tubules of frog skeletal muscle: a confocal fluorescence microscopy study. *J Muscle Res Cell Motil* **16**, 401–411.

Lamb GD, Junankar PR & Stephenson DG (1995). Raised intracellular $[Ca^{2+}]$ abolishes excitation-contraction coupling in skeletal muscle fibres of rat and toad. *J Physiol* **489**, 349–362.

Lannergren J, Bruton JD & Westerblad H (1999). Vacuole formation in fatigued single muscle fibres from frog and mouse. *J Muscle Res Cell Motil* **20**, 19–32.

McArdle A, Edwards RH & Jackson MJ (1995). How does dystrophin deficiency lead to muscle degeneration? – Evidence from the mdx mouse. *Neuromuscul Disord* **5**, 445–456.

McNally EM, de Sa Moreira E, Duggan DJ, Bonnemann CG, Lisanti MP, Lidov HG, Vainzof M, Passos-Bueno MR, Hoffman EP, Zatz M & Kunkel LM (1998). Caveolin-3 in muscular dystrophy. *Hum Mol Genet* **7**, 871–877.

Maughan DW & Godt RE (1999). Parvalbumin concentration and diffusion coefficient in frog myoplasm. *J Muscle Res Cell Motil* **20**, 199–209.

Nagerl UV, Novo D, Mody I & Vergara JL (2000). Binding kinetics of calbindin-D (28k) determined by flash photolysis of caged Ca^{2+}. *Biophys J* **79**, 3009–3018.

Novo D, DiFranco M & Vergara JL (2003). Comparison between the predictions of diffusion-reaction models and localized Ca^{2+} transients in amphibian skeletal muscle fibers. *Biophys J* **85**, 1080–1097.

Parry DJ & Parslow HG (1981). Fiber type susceptibility in the dystrophic mouse. *Exp Neurol* **73**, 674–685.

Petrof BJ, Stedman HH, Shrager JB, Eby J, Sweeney HL & Kelly AM (1993). Adaptations in myosin heavy chain expression and contractile function in dystrophic mouse diaphragm. *Am J Physiol* **265**, C834–C841.

Pusch M & Neher E (1988). Rates of diffusional exchange between small cells and a measuring patch pipette. *Pflugers Arch* **411**, 204–211.

Quinlan JG, Johnson SR, McKee MK & Lyden SP (1992). Twitch and tetanus in mdx mouse muscle. *Muscle Nerve* **15**, 837–842.

Raymackers JM, Gailly P, Schoor MC, Pette D, Schwaller B, Hunziker W, Celio MR & Gillis JM (2000). Tetanus relaxation of fast skeletal muscles of the mouse made parvalbumin deficient by gene inactivation. *J Physiol* **527**, 355–364.

Rayns DG, Simpson FO & Bertaud WS (1968). Surface features of striated muscle. II. Guinea-pig skeletal muscle. *J Cell Sci* **3**, 475–482.

Revel JP (1962). The sarcoplasmic reticulum of the bat cricothyroid muscle. *J Cell Biol* **12**, 571–588.

Sacco P, Jones DA, Dick JR & Vrbova G (1992). Contractile properties and susceptibility to exercise-induced damage of normal and mdx mouse tibialis anterior muscle. *Clin Sci (Lond)* **82**, 227–236.

Simon BJ, Klein MG & Schneider MF (1991). Calcium dependence of inactivation of calcium release from the sarcoplasmic reticulum in skeletal muscle fibers. *J Gen Physiol* **97**, 437–471.

Song L-S, Sham JSK, Stern MD, Lakatta EG & Cheng H (1998). Direct measurement of SR release flux by tracking 'Ca spikes' in rat cardiac myocytes. *J Physiol* **512**, 677–691.

Szentesi P, Jacquemond V, Kovacs L & Csernoch L (1997). Intramembrane charge movement and sarcoplasmic calcium release in enzymatically isolated mammalian skeletal muscle fibres. *J Physiol* **505**, 371–384.

Turner PR, Fong PY, Denetclaw WF & Steinhardt RA (1991). Increased calcium influx in dystrophic muscle. *J Cell Biol* **115**, 1701–1712.

Turner PR, Westwood T, Regen CM & Steinhardt RA (1988). Increased protein degradation results from elevated free calcium levels found in muscle from mdx mice. *Nature* **335**, 735–738.

Tutdibi O, Brinkmeier H, Rudel R & Fohr KJ (1999). Increased calcium entry into dystrophin-deficient muscle fibres of MDX and ADR-MDX mice is reduced by ion channel blockers. *J Physiol* **515**, 859–868.

Vergara JL & Bezanilla F (1981). Optical studies of E-C coupling with potentiometric dyes. In *The Regulation of Muscle Contraction: Excitation-Contraction Coupling*, ed. Brazier AGM, pp. 66–77. Academic Press, Inc., New York.

Vergara JL, Delay M, Heiny JA & Ribalet B (1983). Optical studies of T-system potential and calcium release in skeletal muscle fibers. In *The Physiology of Excitable Cells*, ed. Grinnell AD & Moody WJ, pp. 343–355. Alan R. Liss, Inc., New York.

Vergara J & DiFranco M (1992). Imaging of calcium transients during excitation-contraction coupling in skeletal muscle fibers. *Adv Exp Med Biol* **311**, 227–236.

Vergara JL, DiFranco M & Novo D (2001). Dimensions of calcium release domains in frog skeletal muscle fibers. *SPIE Proc* **4259**, 133–143.

Watchko JF, O'Day TL & Hoffman EP (2002). Functional characteristics of dystrophic skeletal muscle: insights from animal models. *J Appl Physiol* **93**, 407–417.

Williams DA, Head SI, Lynch GS & Stephenson DG (1993). Contractile properties of skinned muscle fibres from young and adult normal and dystrophic (mdx) mice. *J Physiol* **460**, 51–67.

Wood DS, Sorenson MM, Eastwood AB, Charash WE & Reuben JP (1978). Duchenne dystrophy: abnormal generation of tension and Ca++ regulation in single skinned fibers. *Neurology* **28**, 447–457.

Woods CE, Novo D, DiFranco MG & Vergara JL (2004). The action potential evoked sarcoplasmic reticulum calcium release is impaired in mdx mouse muscle fibers. *J Physiol* **557**, 59–75.

Zampighi G, Vergara J & Ramon F (1975). On the connection between the transverse tubules and the plasma membrane in frog semitendinosus skeletal muscle. Are caveolae the mouths of the transverse tubule system? *J Cell Biol* **64**, 734–740.

Acknowledgements

We thank Mr B. Criswell for help with muscle fibre preparation and Dr G. Faas for help with *in vitro* $[Ca^{2+}]$ calibrations. C.E.W. was partially supported by National Institutes of Health Training Grant GM08042 (UCLA MSTP). This work was supported by National Institutes of Health grants AR25201 and AR47664, and a Grant in Aid from the Muscular Dystrophy Association, to J.L.V., and a National Science and Engineering Research Council fellowship PGSB-242387-2001, Canada, to D.N.

Authors' present addresses

C. E. Woods: MSTP, UCLA School of Medicine, Los Angeles, CA 90095, USA.

D. Novo: deNovo Software, Culver City, CA 90232, USA.